Article:
Pedro, RDO, Pereira, S, Goycoolea, FM et al. (2 more authors) (2018) Self-aggregated nanoparticles of N-dodecyl,N′-glycidyl(chitosan) as pH-responsive drug delivery systems for quercetin. Journal of Applied Polymer Science, 135 (2). 45678. ISSN 0021-8995

https://doi.org/10.1002/app.45678

Self-aggregated nanoparticles of N-dodecyl,N'-glycidyl(chitosan) as pH-responsive drug delivery systems for quercetin

Rafael de Oliveira Pedro[a,b], Susana Pereira[b], Francisco M. Goycoolea[b,c], Carla C. Schmitt [a], Miguel G. Neumann*[a]

[a]Instituto de Química de São Carlos, Universidade de São Paulo, Caixa Postal 780, 13560-970 São Carlos, SP, Brazil

[b]Institute of Plant Biology and Biotechnology (IBBP), Westfälische Wilhelms-Universität Münster, Schlossgarten 3, Münster 48149, Germany

[c]School of Food Science and Nutrition, University of Leeds, Leeds LS2 9JT, United Kingdom

E-mail address: neumann@iqsc.usp.br (M.G. Neumann).

ABSTRACT

In this study, pH-responsive amphiphilic chitosan (CS) nanoparticles were used to encapsulate quercetin (QCT) for sustained release in cancer therapy. The novel CS derivatives were obtained by synthesis with 2,3-epoxy-1-propanol, also known as glycidol, followed by acylation with dodecyl aldehyde. Characterization was performed by spectroscopic, viscosimetric, and size-determination methods. Critical aggregation concentration, morphology, entrapment efficiency, drug release profile, cytotoxicity, and hemocompatibility studies were also carried out. The average size distribution of the self-assembling nanoparticles measured by dynamic light scattering ranged from 140 to 300 nm. *In vitro* QCT release and Korsmeyer–Peppas model indicated that pH had a major role in drug release. Cytotoxicity assessments indicated that the nanoparticles were non-cytotoxic. 3-(4,5-Dimethylthiazol-2-yl)-2,5-diphenyltetrazolium bromide assay further revealed that QCT-loaded nanoparticles could inhibit MCF-7 cell growth. *In vitro* erythrocyte-induced hemolysis indicated the good hemocompatibility of the nanoparticles. These results suggest that the synthesized copolymers might be potential carriers for hydrophobic drugs in cancer therapy.
 J. Appl. Polym. Sci. 2018, *135*, 45678.

INTRODUCTION

Chitosan (CS) is a natural polymer that can be extracted from exoskeletons of insects and crustaceans. Due to its low toxicity, biodegradability, and biocompatibility,1-3 many biological applications have been reported for CS, including tissue engineering for cell cultures,4-6 wound healing,7, 8 gene9-11 and drug delivery,12, 13 antibacterial14, 15 and antifungal activities.16-19 Due to its ability to self-assemble in solution forming nanoparticles, amphiphilic derivatives of CS are widely used in many biological applications, such as carriers for genes, proteins, and drugs.20, 21 Normally, amphiphilic derivatives are obtained by the addition of hydrophilic and hydrophobic groups to the polymer backbone. This modification increases the intra- and intermolecular interactions responsible for the aggregation process.

Nanotechnology has emerged as a potential tool in cancer therapy. Advances in materials science and cancer biology have contributed to improved therapeutic systems. Nanoscale

carriers can selectively release drugs into the tumor regions by exploring specific characteristics of the cancerous tissues, reducing side effects on healthy cells. These characteristics include leaky vasculature, angiogenesis, presence of specific enzymes, pH changes, among others.[22-24] pH-sensitivity polymers, such as CS, can be used as carriers for cancer therapy, since fermentative glycolysis in cancer tissues might lead to acidic conditions in the extracellular region decreasing the local pH to values as low as 5.0.[25-27] After reaching these regions, the carrier systems may release the drug by responding to pH changes in the extracellular fluids of the tumor tissues.

The CS backbone can be protonated/deprotonated according to the pH of the medium being below or above its pK_a (≈6.4), respectively.[28] This characteristic gives this polymer pH sensitivity, since the properties and structure of CS change according to its protonation. Therefore, it is possible to use amphiphilic derivatives as pH-sensitive drug carriers in cancer therapy. Although studies involving amphiphilic CS have been undertaken to produce derivatives with improved self-assembling characteristics, biological properties of these systems need to be optimized. In cancer treatment, carriers should have low cytotoxicity, good hemocompatibility, and adequate specificity for tumor regions.

Epoxide derivatives are widely used reagents due to their very reactive groups.[29] The structure of this cyclic ether is an equilateral triangle with bond angles of 60° and slight differences in electronegativity are due to the carbon–oxygen bonds. This makes these compounds powerful electrophiles that can react with nucleophiles, such as the amine groups present in the CS backbone. The small 2,3-epoxy-1-propanol molecule, also known as glycidol (GLY), containing epoxide and hydroxyl functional groups was used as a hydrophilic grafting agent to modify CS.

In this research, a novel amphiphilic co-polymer was synthesized by grafting GLY to the CS backbone, followed by reductive alkylation with different amounts of dodecyl aldehyde (DDA) (Figure 1). The derivatives were characterized by ^{1}H nuclear magnetic resonance (NMR), attenuated total reflectance-Fourier transform infrared spectroscopy (ATR-FTIR), and ultraviolet–visible (UV–vis) spectroscopy. The behavior of the self-assembled amphiphilic derivatives in aqueous solution was determined by fluorescence spectroscopy. Dynamic light scattering (DLS) was used to monitor average size and ζ-potential of the particles. The release of quercetin (QCT) from the nanoparticles was investigated at different pHs. Cytotoxicity studies and hemocompatibility were carried out to ensure the conditions for biological application.

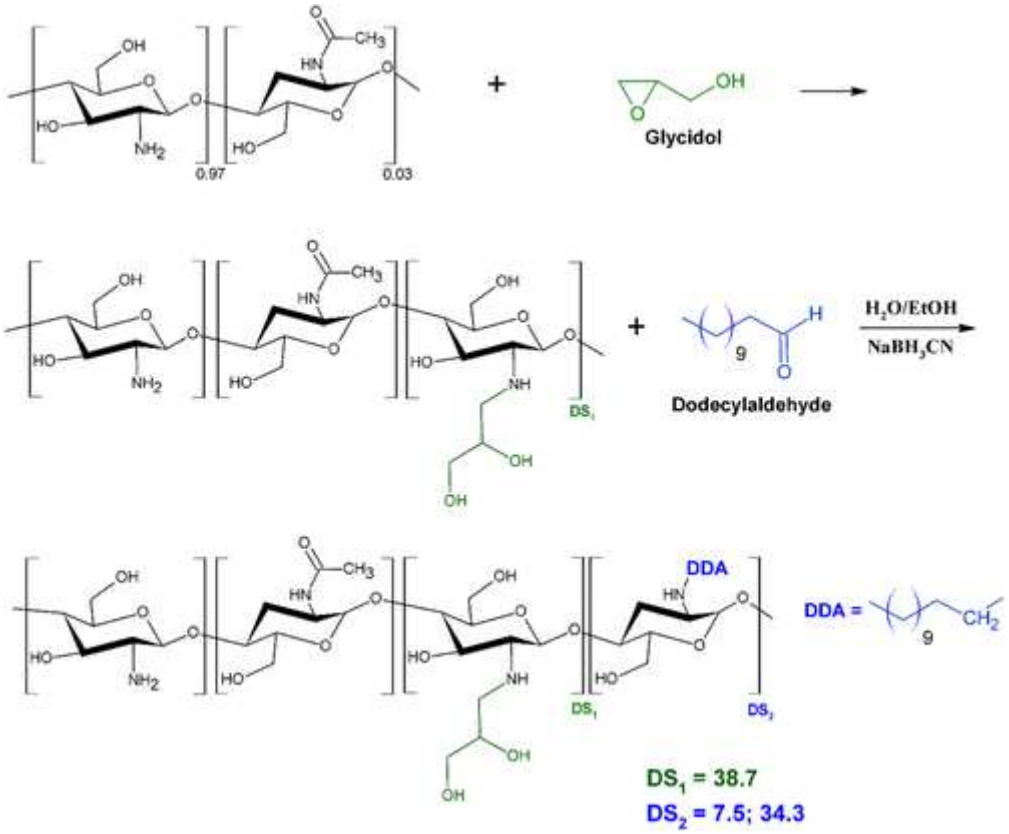

Figure 1

Schematic representation of the synthesis of the amphiphilic derivatives of CS.

EXPERIMENTAL

Materials

CS powder [low-molecular weight, deacetylation degree (DD) ≥ 85%], GLY, DDA, sodium hydroxide, sodium acetate, acetic acid, and pyrene were reagent grade and used as received from Sigma Aldrich Chemical Co., Brazil. 3-(4,5-Dimethylthiazol-2-yl)-2,5-diphenyltetrazolium bromide (MTT) and RPMI-1640 cell culture medium were purchased from Sigma-Aldrich GmbH, Germany. Ultrapure MilliQ water was used throughout.

Deacetylation of CS

Deacetylated CS (D-CS) was prepared in aqueous NaOH solution as described earlier.30 Briefly, commercial CS powder (C-CS) (12.0 g, 7.44×10^{-2} mol of monosaccharide units) was dissolved in aqueous acetic acid (400 mL, 2 wt %) for 12 h to ensure the complete solubilization. Subsequently, this solution was added drop-wise to aqueous NaOH (200 mL, 50 wt %) at room temperature. The suspension was allowed to react in nitrogen atmosphere at 105 °C for 1.5 h. After the reaction time, the suspension was filled with preheated water at 60 °C up to 4 L. Subsequently, the precipitate was washed five times with water, separated by filtration, and the procedure was repeated to achieve a higher DD. The polymer was

isolated by lyophilization after purification by dialysis against water for 5 days (yield 11.1 g, 92.5%). The DD of the *N*-D-CS was calculated using the integrals of the peaks of the ^{1}H-NMR spectra corresponding to the protons of the *N*-acetyl group at 2.3 ppm and the peak due to the C2 proton at 5.3 ppm.31

Depolymerization of CS

The depolymerization of CS was carried out by oxidation with sodium nitrate in acid solution using the procedure described by Tommeraas *et al*.32 Approximately, 10.0 g of previously D-CS were solubilized in 555 mL of acetic acid solution (2 wt %) for 12 h. Then the solution was purged with nitrogen for 1 h under constant stirring and cooled at 4 °C. Afterward, the stirring was stopped and 18.6 mL of aqueous sodium nitrite (231 mg) was added to the mixture and the reaction was kept at 4 °C for 18 h in the absence of light. After this reaction time, the resulting solution was precipitated with sodium hydroxide and centrifuged at 10,000 rpm. The precipitate was then washed with deionized water and the obtained product was lyophilized.

Syntheses

GLY-Modified CS

Hydrophilic CS grafted with GLY was prepared by dispersing 6.0 g (3.72×10^{-2} mol) of CS in aqueous acetic acid (300 mL, 2 wt %). After complete solubilization, 9.5 mL of GLY were added drop-wise to the solution and the mixture was refluxed at 50 °C for 24 h. The polymer was purified by dialysis against water, isolated by lyophilization and characterized by ^{1}H-NMR and ATR-FTIR.

Preparation of Amphiphilic CS

Amphiphilic derivatives were obtained by the previously described method.33 Briefly, GLY-modified CS (3.0 g, 1.2×10^{-2} mol), dissolved in acetic acid (0.2 *M*, 330 mL), was added drop-wise to ethanol (240 mL). Afterwards, different amounts of DDA dissolved in ethanol (10 mL) were added and the mixture was stirred for 1 h at room temperature. Sodium cyanoborohydride was added and the solution was allowed to react for 24 h under stirring at room temperature. The final product was purified by dialysis against water for 3 days, isolated by lyophilization and characterized by ^{1}H-NMR and ATR-FTIR.

Characterization Methods

Viscosity

Molar masses were determined from intrinsic viscosities measured using a digital rolling-ball viscometer (Lovis 2000 MME, Anton Paar, Graz, Austria). Measurements were made at concentrations in the $3.0–7.0 \times 10^{-3}$ g/mL range at pH 4.5 using an acetic acid (0.3 *M*)/sodium acetate (0.2 *M*) buffer. The average viscosimetric molecular weights of C-CS, D-CS, and

depolymerized low-molecular-weight CS (L-CS) were determined from the intrinsic viscosities, η, using the Mark–Houwink equation and the constants, a = 0.76 and K = 0.076 mL/g for C-CS and, a = 0.82 and K = 0.076 mL/g for D-CS and L-CS, as suggested by Rinaudo *et al*.34

^{1}H-NMR Spectroscopy

Samples were prepared by dissolution of ∼10 mg of CS samples in 1 mL of deuterium oxide (D_2O) and 10 µL of deuterium chloride. After complete solubilization, the ^{1}H-NMR spectra were recorded on an Agilent 400/54 Premium Shielded spectrometer at 70 °C.

ATR-FTIR Analysis

ATR-FTIR analysis (Perkin Elmer Frontier FTIR spectrometer, Perkin Elmer, Shelton, CT) was performed on freeze-dried samples to confirm the occurrence of the reaction between CS and GLY and DDA. All spectra were recorded at room temperature and four scans were averaged over the of 4000–600 cm^{-1} range.

Derivatives Solubility

The transmittance of the derivatives samples at 550 nm (wavelength at which CS does not absorb) was used to monitor the solubility as function of the pH. Approximately, 20 mg of the samples were dissolved in 20 mL of acetic acid (0.10 *M*).31 After complete solubilization, portions of NaOH (25 µL, 0.5 *M*) were added to the solution up to pH 12. The pH was measured with a UB-10 pH-meter (Denver Instrument, Bohemia, NY) and the transmittance was recorded on a UV-2550 ultraviolet–visible spectrophotometer (Shimadzu, Kyoto, Japan).

Critical Aggregation Concentrations

Fluorescence measurements were recorded on a Hitachi F4500 spectrophotometer using pyrene as a hydrophobic fluorescence probe to measure the self-aggregation behavior of the derivatives.2 Pyrene, dissolved in methanol (1×10^{-3} *M*) was added to solutions of the derivatives (1.0 g/L) in order to obtain 5.0×10^{-6} *M* solutions of the probe. The I_1/I_3 ratio between the first (373 nm) and the third (382 nm) vibronic peaks of the probe fluorescence was used to evaluate the local environment polarity of the nanoparticles. Pyrene was excited at 310 nm and its emission spectra were recorded from 350 to 500 nm.

Particle Size Distribution and Zeta Potential

The size distribution of the particles were determined using DLS with non-invasive back scattering (DLS-NIBS) at an angle of 90°. The zeta (ζ)-potential was measured by mixed laser Doppler velocimetry and phase analysis light scattering (M3-PALS). A Malvern Zetasizer NanoZS (Malvern Instruments Ltd., Worcestershire, UK) fitted with a red laser (λ = 632.8 nm)

at 25 °C was used to conduct both determinations. Derivative solutions were prepared at concentration 0.1–1.0 g/L, at pH 5.0 (acetate buffer) and 7.4 (phosphate buffer).

Transmission Electron Microscopy Observation

A JEM2100 LaB6 (Jeol, Japan) transmission electron microscope operating at 200 keV was used to assess the surface morphology of the nanoparticles. The sample solution (0.5 mg/mL, 20 µL) was placed onto the carbon-coated 200 mesh copper grid and air-dried for 20 min. Afterwards, the grids were stained with phosphotungstic acid at 2% and dried at room temperature before transmission electron microscopy (TEM) observations.

Evaluation of QCT Loading and Release

QCT-loaded nanoparticles were prepared using a centrifugation method. Briefly, 20 mg of sample were dispersed in 3 mL of sodium acetate buffer (pH 5.0). After gentle stirring for 8 h, ethanolic QCT solutions were added and the mixture was allowed to stir for another 4 h in the dark. Centrifugation (15,000 rpm for 50 min at 15 °C) was used to isolate the QCT-loaded nanoparticles. The free QCT concentration in the supernatant was determined by UV–visible spectrophotometry. The entrapment efficiency (EE) and the drug loading (DL) efficiency were calculated using

$$\mathrm{EE}(\%) = \frac{(\text{total drug weight} - \text{free drug weight})}{(\text{total drug weight})} \times 100\% \quad (1)$$

$$\mathrm{DL}(\%) = \frac{(\text{total drug weight} - \text{free drug weight})}{(\text{loaded drug weight} + \text{nanoaggregates weight})} \times 100\% \quad (2)$$

Sodium acetate buffer (pH 5.0) and phosphate buffer saline (PBS, pH 7.4) were used as media for the QCT release studies. The centrifuged nanoparticles were re-suspended in the desired buffer solution and transferred to a Pur-A-Lyzer Mini Dialysis Kit (MWCO 6–8 kDa). The dialysis tubes were immersed in 35 mL of the corresponding buffer solution, under gentle stirring at 37 ± 0.5 °C. At the sampling times, 3 mL of the release media were collected for evaluation of the amount of released QCT using UV–visible spectrophotometry.35 An equal volume of fresh buffer was replaced in the solution after each withdrawal.

The drug release mechanism from nanoparticles was evaluated using the Korsmeyer–Peppas model [eq. 3]36, 37

$$\frac{M_t}{M_\infty} = kt^n \quad (3)$$

where M_t is the mass of QCT released at time t, M_∞ is the total mass of QCT to be released, and k is a constant dependent on the structural characteristics of the nanoparticles, solvent, and material interactions. The diffusion, represented by the exponent n, is considered Fickian when n = 0.43 and case II transport when n = 0.85. Anomalous diffusion takes place when n is between these values. When n > 0.85 the diffusion involves super-case II transport. Fickian diffusion can also happen when n is lower than 0.43, if the system is polydispersed with spherical particles.38 The model was applied for release up to M_t/M_∞ < 0.6.

Cytotoxicity Assay

The effects of the free QCT, blank, and loaded nanoparticles on the viability of human breast cancer cells (MCF-7) were evaluated using the MTT assay. Cells were seeded in the 96-well plate at a density of ∼104 cells per well (or ∼105 cells/mL) and cultured for 24 h (RPMI 1640 medium (Sigma-Aldrich) supplemented with 10% (vol/vol) fetal bovine serum, 1% (vol/vol) l-glutamine (200 mM) and 1% (vol/vol) penicillin–streptomycin (10,000 units penicillin, 10,000 units of streptomycin in 0.9% NaCl). Each well was washed with supplement-free medium before adding the sample. After an additional incubation with different concentrations of the samples, the wells were washed twice with supplement-free medium. Immediately, 100 µL of the medium and 25 µL of MTT solution in PBS (5 mg/mL) were added to each well. After further incubation for 4 h, the dye was solubilized with 150 µL of dimethylsulphoxide (DMSO) using orbital shaking at 300 rpm for 15 min. A microplate reader (Safire, Tecan AG, Salzburg, Austria) was used to measure the absorbance at 570 nm. Relative viability (%) values were calculated according to the absorbance ratio of the wells treated with samples and wells containing untreated cells (negative control). 4% Triton X-100 in PBS solutions was used as positive control. All experiments were carried out as independent triplicates on different days to determine averages and standard deviations.

Blood Compatibility Assessments

The hemocompatibility tests were performed by diluting 800 µL of freshly collected pig blood with 1 mL of PBS buffer. Approximately 20 µL of diluted blood were added to1 mL of nanoparticles dispersed in PBS (1 mg/mL) and incubated for 60 min at 37 °C. Afterward, the hemolysis ratio (HR) was calculated using the absorbance of the samples at 545 nm in the following equation

$$\mathrm{HR}(\%) = \frac{A_{\mathrm{sample}} - A_{\mathrm{PBS}}}{A_{\mathrm{water}} - A_{\mathrm{PBS}}} \times 100\% \qquad (4)$$

where A_{sample}, A_{PBS}, and A_{water} are the absorbance at 545 nm of blood samples treated with nanoparticles, PBS (negative control), and water (positive control), respectively. All the hemocompatibility experiments were done in triplicate.

RESULTS AND DISCUSSION

Characterization of the Amphiphilic Derivatives

Regardless of its advantages, the poor solubility of CS in water has been a crucial barrier to its modification and applications. To improve its solubility, a novel water-soluble GLY-grafted CS was synthesized. In addition, this hydrophilic CS was further modified with the hydrophobic group DDA in order to improve the amphiphilic character of the samples, which can self-assemble in aqueous solution. It is also known that the molecular weight of the CS is an essential factor affecting the self-assembling process, since long CS chains can obstruct the movement of the backbone during the procedure.28 Therefore, to optimize the assembling properties, the D-CS was depolymerized before further modifications. The molecular weight for C-CS, D-CS, and deacetylated with L-CS are shown in Table 1.

Table 1. Amphiphilic Derivatives Characterization and Viscosity-Average Molecular Weight

Sample	DD[a] (%)	DS_1[b] (%)	DS_2[c] (%)	M_v (kDa)
C-CS	84.3	—	—	82.4
D-CS	97.1	—	—	50.4
L-CS	97.1	—	—	3.8
L-CS-GLY_{40}	—	38.7	—	—
L-CS-$GLY_{40}D_7$	—	38.7	7.5	—
L-CS-$GLY_{40}D_{34}$	—	38.7	34.3	—

[a] Deacetylation degree.
[b] Degree of substitution at the hydrophilic chain.
[c] Degree of substitution at the hydrophobic chain.

As shown in Figure 1, GLY-grafted CS was obtained by nucleophilic substitution of the C-2 amine groups with GLY. The final product was characterized by ^{1}H-NMR and FTIR to confirm the presence of the chemical bonds of the substituents. L-CS sample was used as starting material.

^{1}H-NMR spectra [Figure 2(a,b)] were used to calculate the DD of the derivatives. The areas corresponding to acetamido methyl protons (δ = 2.35 ppm) and the doublet corresponding to

the resonance of the anomeric proton at δ = 5.21 ppm were used in eq. 5.39 The DD, expressed in —NH2 mol %, was 84.3% for C-CS and 97.1% for D-CS and L-CS.

$$DD(\%) = \left[1 - \left(\frac{I_{2.35}}{3I_{5.20}}\right)\right] \times 100\% \qquad (5)$$

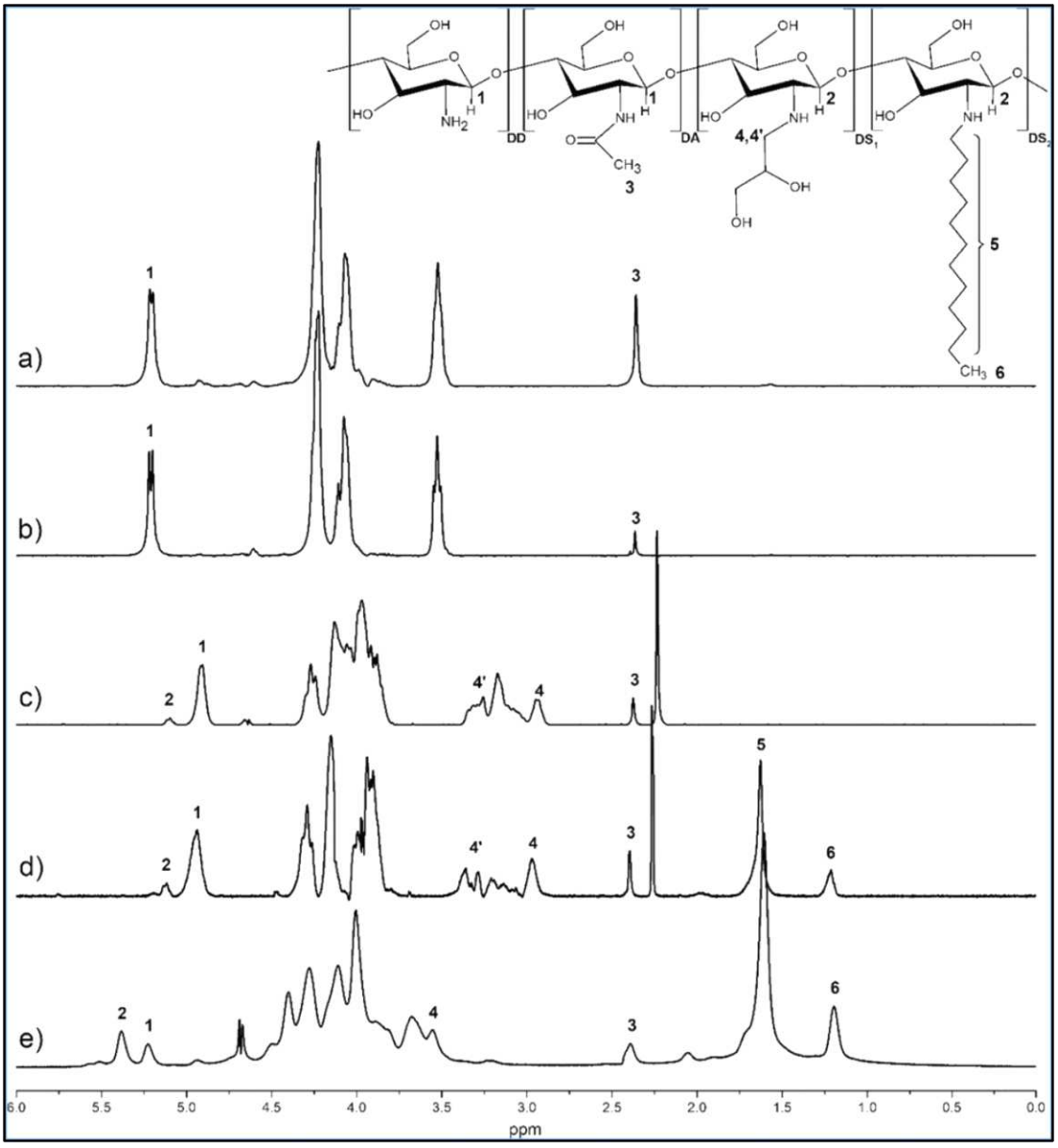

Figure 2
^{1}H-NMR spectra of (a) C-CS, (b) deacetylated L-CS, (c) the hydrophilic derivative containing 38.7% of GLY (L-CS-GLY_{40}), and its amphiphilic derivatives containing (d) 38.7% of hydrophilic groups and 7.5% of the hydrophobic chain (L-CS-$GLY_{40}D_7$) and (e) 38.7% of hydrophilic groups and 34.3% of the hydrophobic chain (L-CS-$GLY_{40}D_{34}$).

The degree of substitution by the reaction with GLY (DS_1) was calculated from the ^{1}H-NMR spectra of the CS derivative [Figure 2 (c)]. The broad peaks at δ = 2.97 ppm and δ = 3.26 ppm can be attributed to protons bonded to the carbons of the —C**H$_2$**OH group in the *N*-(2,3-dihydroxypropyl) moieties (—C**H$_2$**CHOHCH$_2$OH). The DS_1 was estimated based on the comparison of the peak areas at δ = 2.97 ppm with that of the anomeric protons at δ = 4.91 ppm and δ = 5.10 ppm. Using eq. 6 the degree of substitution DS_1 of L-CS-GLY$_{40}$ could be calculated as being 38.7%.

$$DS_1(\%) = \left[\left(\frac{I_{2.97}}{2(I_{4.91}+I_{5.10})}\right)\right] \times 100\% \qquad (6)$$

The degree of substitution (DS_2) by the hydrophobic dodecyl group (DDA) was calculated using eq. 7 and the areas at δ = 1.21 ppm attributed to resonance of the protons of the methyl group present in the C12 chain of the DDA substituent, and the anomeric protons at δ = 4.94 ppm and δ = 5.11.30 The signals in the region 1.54 to 1.77 ppm are due to the resonance of methylene hydrogen in the C12 moieties [Figure 2(d,e)].

$$DS_2(\%) = \left[\frac{I_{1.21}}{3(I_{4.94}+I_{5.11})}\right] \times 100\% \qquad (7)$$

The DS_2 for L-CS-GLY$_{40}$D$_7$ was 7.5% and for L-CS-GLY$_{40}$D$_{34}$ was 34.3%. Table 1 shows the DS at different sites of the compounds.
FTIR spectra for deacetylated L-CS, GLY-grafted CS derivative (L-CS-GLY$_{40}$), and the amphiphilic derivatives L-CS-GLY$_{40}$D$_7$ and L-CS-GLY$_{40}$D$_{34}$ are shown in Figure 3.

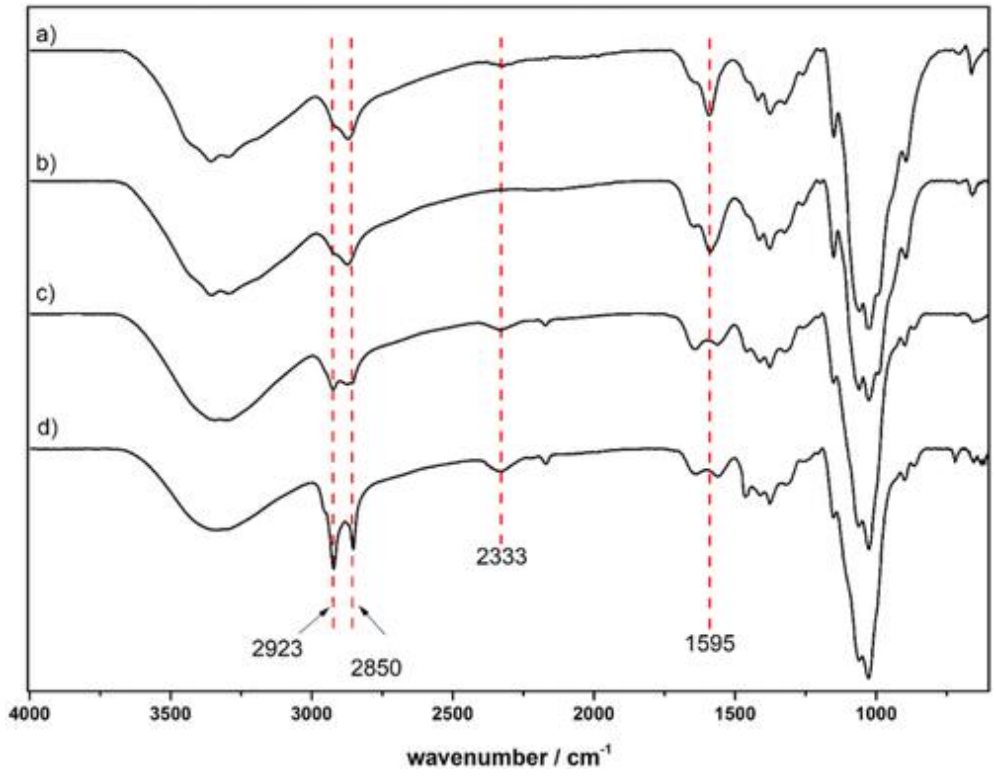

Figure 3
FTIR spectra of (a) deacetylated L-CS, (b) GLY-grafted CS (L-CS-GLY$_{40}$), and its amphiphilic derivatives (c) L-CS-GLY$_{40}$D$_7$ and (d) L-CS-GLY$_{40}$D$_{34}$.

The decrease of the peak intensity around 1595 cm^{-1}, related to the N⍰H bending vibration of the primary amino group, when comparing the FTIR spectra of D-CS [Figure 3(a)] with the derivatives [Figure 3(b–d)], is an evidence that hydrophilic GLY molecule reacted with the primary amine (—NH_2) of the CS chain.40 It is also possible to see that all samples have a characteristic band around 3400 cm^{-1} due to the axial stretching vibration of the hydroxyl groups (O—H) of CS chains and residual free water.41

Characteristic peaks can be seen at 2923 and 2850 cm^{-1} for the amphiphilic samples, corresponding to the axial deformation of the carbon–hydrogen bond of the CH_3 and CH_2 groups, respectively, present in the C12 chain of the dodecyl substituent. The FTIR spectra also show that when increasing the substitution of DDA on CS, the peaks at 2923 and 2850 cm^{-1} become sharper, which indicates indirectly the increase of the substitution by DDA. The peak at 2333 cm^{-1} that can be seen in the L-CS-$GLY_{40}D_7$ and L-CS-$GLY_{40}D_{34}$ spectra is related to the vibration of the DDA-substituted amino groups.42

Behavior in Aqueous Solution

The derivatives modified with hydrophilic (GLY) and hydrophobic (DDA) substituents self-assemble in aqueous solution due to their amphiphilic character. Nonetheless, the high-molecular weight of CS could obstruct the movement of the backbone during the self-assembling process. Therefore, low-molecular-weight L-CS-GLY was selected as the starting material to optimize the assembling properties.

The solubility of L-CS and the amphiphilic compounds were evaluated by monitoring the changes in the transmittance of the solutions as function of pH. It is possible to observe in Figure 4 that the presence of hydrophilic groups in the modified CS increases the solubility of the polymer over the entire range of pH. On the other hand, for the starting unmodified CS L-CS (pK_a ≈ 6.4) the transmittance at 550 nm decreases sharply at pH higher than 6.2, for the L-CS-GLY_{40} sample this transmittance was kept at about 99% over the whole pH range, up to 12. The amphiphilic L-CS-$GLY_{40}D_7$ does not change its transmittance when increasing the pH. On the other hand, for the more substituted amphiphilic derivative L-CS-$GLY_{40}D_{34}$ the transmittance decreased from 88% to 79% when changing from acid to basic media. However, it is much more soluble than the unmodified CS at higher pH. The increase of the hydrophobic substitution (L-CS-$GLY_{40}D_7$ vs. L-CS-$GLY_{40}D_{34}$) results in a lower transmittance, probably due to a more efficient aggregation.

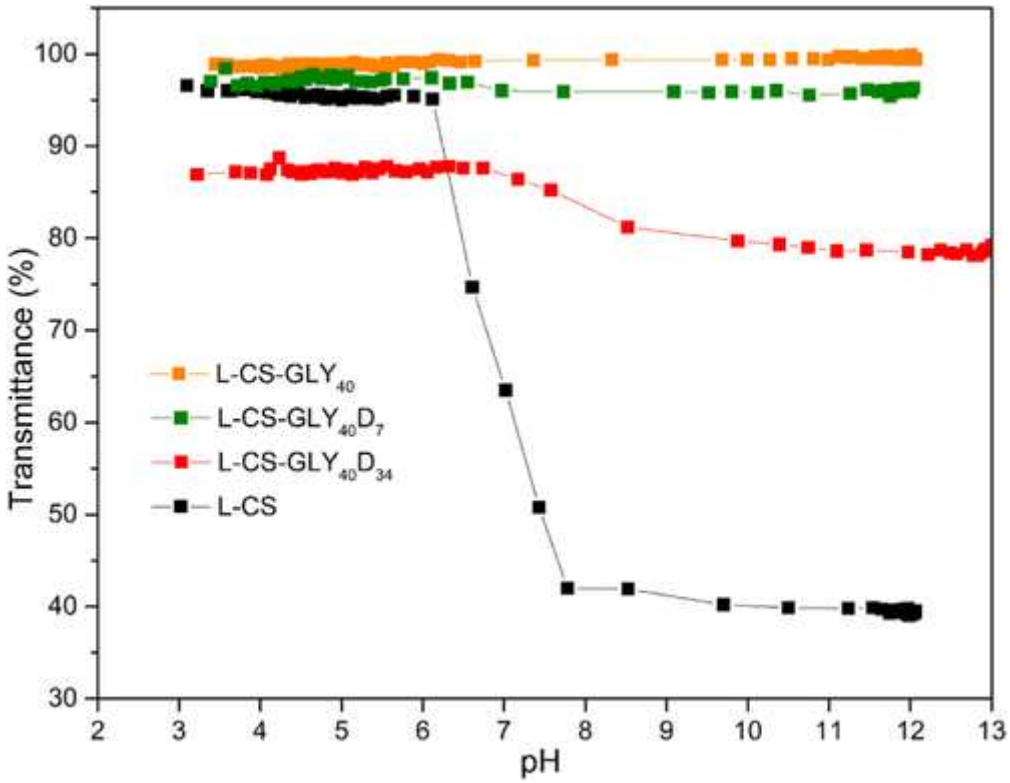

Figure 4
Transmittance versus pH of the derivatives solutions at 550 nm.

The higher solubility of the GLY modified derivatives is due to the presence of two hydroxyl groups in the small glycidyl chain. The formation of hydroxyl–water hydrogen bonds compensates the nonpolar repulsion of the rest of the polymer chain, providing excellent solubility to CS. Although we are using this water-soluble CS to form amphiphilic polymer, it is possible to explore the use of this hydrophilic derivative in other areas such as delivery of DNA and siRNA,43 thermosensitive hydrogel,44 and oral enhancer,45 which corroborates the importance of synthesis described here.

As already shown in a previous work, 30 pyrene can be used as fluorescence probe to track the aggregation behavior of these samples in aqueous solution. This probe does not affect the structure of the aggregates and the I_1/I_3 ratio of the intensity of the fluorescence peaks of pyrene can be correlated with the polarity of the media, which can be used to determine the critical aggregation concentrations (CAC).46 I_1/I_3 ratios in the 2.0–1.3 range indicate that the probe is placed in hydrophilic environments, whereas values below 1.2 indicate a hydrophobic medium.

The CAC values were determined monitoring the variation of the I_1/I_3 ratio of the pyrene peaks intensity with increasing CS concentrations (Supporting Information Figure S1). The pH dependence of the CAC for both amphiphilic derivatives are listed in Table 2. It can be seen that aggregation starts at concentrations in the range 0.003–0.047 g/L and the CAC decreases slightly with the increasing degree of substitution by DDA. That can be explained by the fact that the hydrophobicity increases with higher degree of substitution by the C12 chain, which allows stronger self-aggregation in water solution due to the formation of more compact hydrophobic cores.

Table 2. CAC of the Amphiphilic Derivatives at Different pH

Sample	CAC (g/L × 10^{-3})			
	pH 4.0	pH 5.0	pH 6.2	pH 7.4
L-CS-$GLY_{40}D_7$	47.3	21.6	15.1	4.5
L-CS-$GLY_{40}D_{34}$	36.0	18.1	12.0	3.1

The change with pH can be ascribed to the protonation/deprotonation of the remaining free amino groups of CS that change the electrostatic interaction among the chains, resulting in particles with different properties and CAC.47, 48 No sign of aggregation was observed for the hydrophilic derivative (L-CS-GLY_{40}) even at higher concentrations. This behavior is in agreement with those obtained by solubility measurements (Figure 4).

DLS-NIBS was used to measure the average size of the particles at pH 5.0 and 7.4 (acetate and phosphate buffers, respectively) and the results are shown in Table 3 and Figure 5. The size of the nanoparticles was in the range of 130–300 nm and is similar to those reported in the literature for self-assembled nanoparticles based on CS derivatives.2, 30, 49, 50

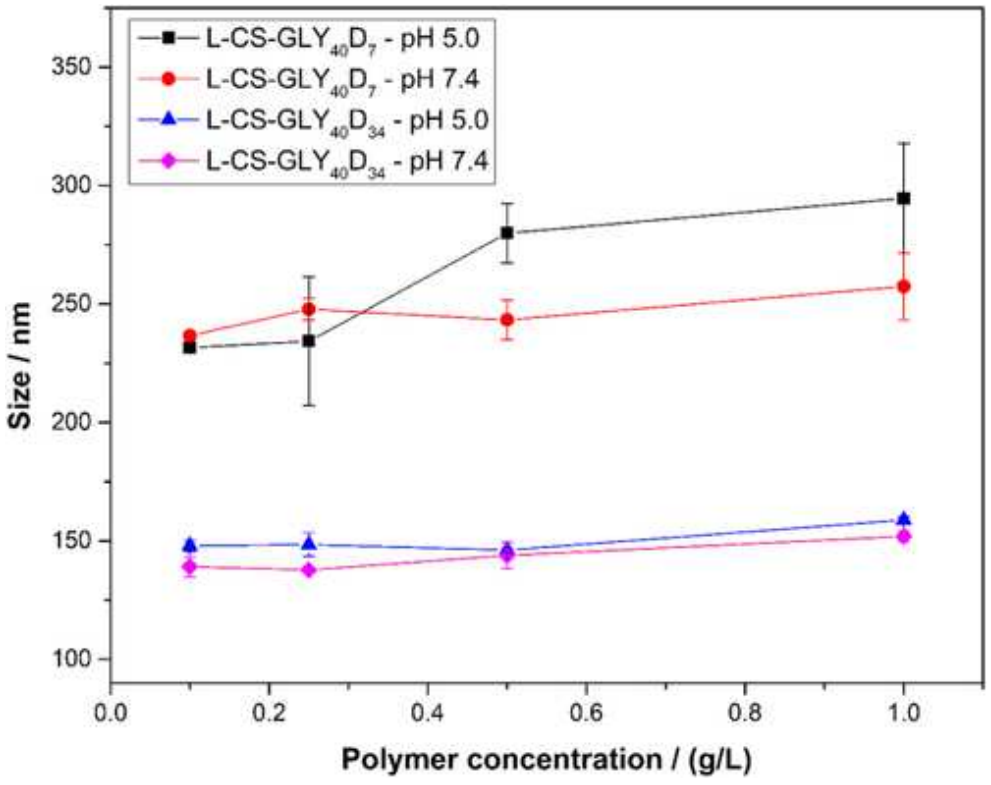

Figure 5
Average size of the particles versus polymer concentrations at pH 5.0 and 7.4.

Table 3. Size and ζ-Potential of the Derivatives at Different pH

	Sample	Concentration (g/L)	Size (d.nm)	Zeta
pH 5.0	L-CS-$GLY_{40}D_7$	0.10	231 ± 2	14.1 ± 1.5
		0.25	234 ± 27	15.6 ± 0.7
		0.50	279 ± 13	17.8 ± 0.6
		1.00	294 ± 23	14.5 ± 0.6
	L-CS-$GLY_{40}D_{34}$	0.10	148 ± 2	20.6 ± 0.2
		0.25	148 ± 3	24.2 ± 0.4
		0.50	146 ± 5	28.8 ± 2.0
		1.00	159 ± 7	29.9 ± 1.8
pH 7.4	L-CS-$GLY_{40}D_7$	0.10	236 ± 1	18.7 ± 1.9
		0.25	247 ± 5	23.4 ± 1.4
		0.50	243 ± 8	28.8 ± 3.2
		1.00	257 ± 14	24.4 ± 0.4
	L-CS-$GLY_{40}D_{34}$	0.10	139 ± 4	22.6 ± 0.9
		0.25	138 ± 5	27.7 ± 0.7
		0.50	144 ± 3	27.8 ± 1.0
		1.00	152 ± 9	30.4 ± 0.3

Values shown correspond to the average of three independent measurements.

The size results show that when the content of the hydrophobic segment was increased (D_7 vs. D_{34}), the particles become smaller and with almost the same average size for all concentrations tested. This phenomenon may be ascribed to the fact that larger substitution by DDA would cause more chains to aggregate, forming more compact hydrophobic cores. Furthermore, it may be noted that at pH 5 the particles formed by the sample L-CS-$GLY_{40}D_7$ at 0.5 and 1.0 g/L have larger diameters due to electrostatic repulsion between the protonated CS chains. On the other hand, with the deprotonation of the polymer at pH 7.4, the particles tend to form more condensed structures. The pH seems to have little influence on the size of the particles formed by the sample L-CS-$GLY_{40}D_{34}$, since they are slightly higher at pH 5.

ζ-potential values (+14.1 to +30.4 mV) suggest that CS chains are in direct contact with the external environment and are relatively stable. The positive charges on the surface of the nanoparticles can increase the biocompatibility of the system, allowing them to be used in biological applications such as drug and gene delivery.[51]

The results shown here are similar to those previously reported30 for the self-assembling of amphiphilic CS quaternary ammonium derivatives. We have shown that both systems (with quaternary ammonium and glycidyl hydrophilic groups) have comparable behavior in aqueous solution and can form particles with a hydrophobic core. However, the derivatives produced by GLY series have lower average diameter, which indicates that they are more stable. We found that the size of nanoparticles, for both self-assembling systems, is influenced by various factors such as pH, concentration, hydrophilic/hydrophobic ratio, and nature of the hydrophilic group. Therefore, it can be concluded that both system may have specific self-assembling characteristics, which allows them to be used in different kinds of applications.

Nanoparticles morphology was further investigated using TEM images (Figure 6). It was evident that the particles have spherical morphology, without significant aggregation among them, with sizes within the range determined by DLS. The differences in the diameters obtained by both techniques are due to the presence of water in the measurements by DLS, whereas TEM measurements are made with dried particles.

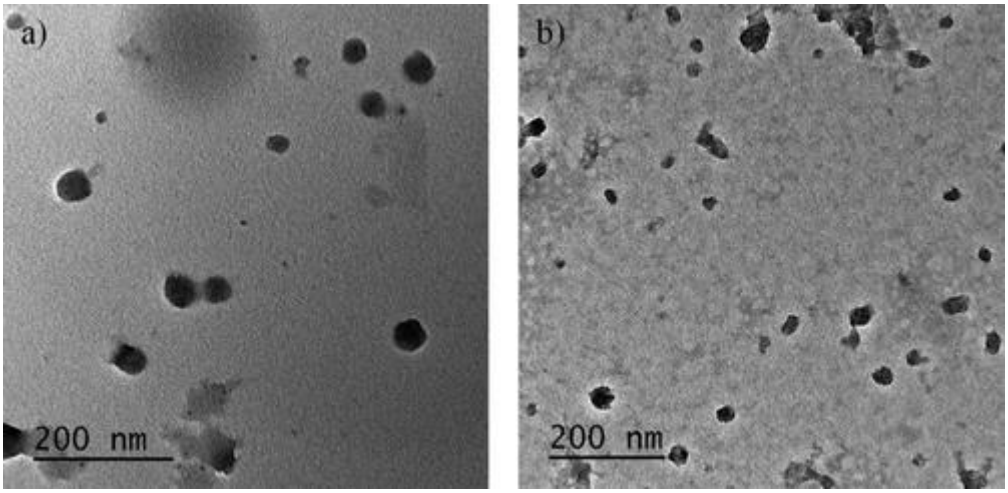

Figure 6
Representative TEM images of blank nanoparticles of (a) L-CS-$GLY_{40}D_7$ and (b) L-CS-$GLY_{40}D_{34}$ at 0.5 mg/mL.

DL and Release Studies

Self-assembled nanoparticles can improve drug bioavailability and release profile in a sustained way. The hydrophobic compound QCT was loaded into the cores of the L-CS-GLY nanoparticles and the EE was determined using UV/vis spectroscopy. The EE was 73.2% for L-CS-$GLY_{40}D_7$ and 77.7% for L-CS-$GLY_{40}D_{34}$. On the other hand, the DL decreased from 5.2% to 4.3% for L-CS-$GLY_{40}D_7$ and L-CS-$GLY_{40}D_{34}$, respectively. As can be expected, the increase in the substitution by the DDA group promotes the increase of EE, due to the presence of more hydrophobic sites for interaction with QCT. The EE and DL for these samples are superior to those reported in similar studies.52-54 In spite of these observations, it is necessary to emphasize that the encapsulation process is complex and can be influenced by several

factors, including CS molar mass, hydrophobic chain length, chemical drug structure, and drug–solvent interactions.

The QCT release profiles at pH 5 and 7.4 are shown in Figure 7. As can be seen, there is a burst release effect during the first 8 h, probably due to weakly attached QCT on the surface of the nanoparticles. This step is followed by a constant release thereafter. For the L-CS-$GLY_{40}D_7$ nanoparticle, after 96 h the drug release at pH 5 reached 82% and 60% at pH 7.4. A similar behavior was observed for the L-CS-$GLY_{40}D_{34}$ sample, with maximum release of 65% and 27% at pH 5 and 7.4, respectively. The electrostatic repulsion and formation of hydrogen bonds between water molecules and the protonated amino groups at pH 5 facilitates the diffusion and release of the QCT, while the absence of protonation at pH 7.4 reduces the amount of drug released.

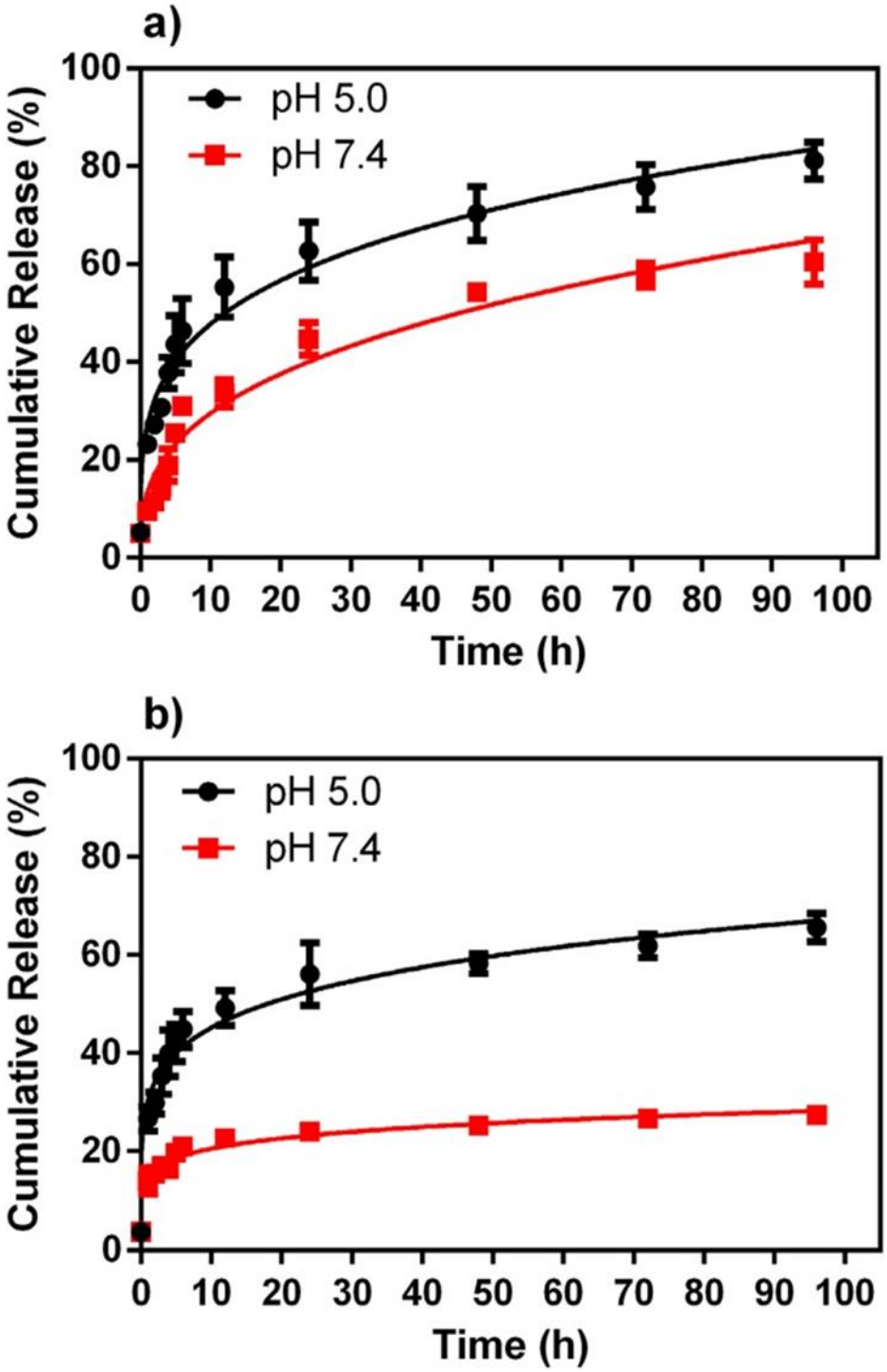

Figure 7
In vitro release profile of QCT from (a) L-CS-$GLY_{40}D_7$ and (b) L-CS-$GLY_{40}D_{34}$ at pH 5.0 and 7.4 and 37 °C.

The substitution by the C12 chain has also an important role over the release. While the L-CS-$GLY_{40}D_7$ sample shows a lower EE, it has larger maximum release when compared to L-CS-$GLY_{40}D_{34}$. This behavior may be ascribed to the interactions among the C12 chain and the hydrophobic QCT. The sample L-CS-$GLY_{40}D_7$ has fewer hydrophobic chains, thus QCT is weakly encapsulated in this sample. This explains why at pH 5 the sample L-CS-$GLY_{40}D_7$ has maximum release of 82% against 60% for the L-CS-$GLY_{40}D_{34}$ sample.

In addition to the higher encapsulation capacity and pH sensitivity, the longer sustained release period is one of the main advantages of the carriers developed here. Other studies usually show nanocarriers promoting the release of drugs for 6,[55] 24,[56] or 72 h,[57] while our system allows sustained release for up to 96 h. Moreover, maintaining the drug's therapeutic levels for longer periods requires fewer applications during the treatment, reducing possible side effects of the drugs.

The mathematical Korsmeyer–Peppas model was used to evaluate the release of QCT. This model has been widely used to characterize drug release mechanisms from spherical nanoparticles.[13, 56, 58, 59] The fitting data (Table 4) revealed strong dependence on the pH, suggesting that there is a change in the outer layer of the nanoparticles as function of pH. These results indicate that there is influence of the medium on the structural characteristics of the nanoparticles.

Table 4. Mathematical Parameters of the Release Data

Sample	pH	*K*	*N*	Correlation value (R^2)	Type of diffusion
L-CS-$GLY_{40}D_7$	5.0	20.7 ± 2.2	0.44 ± 0.01	0.9717	Anomalous
	7.4	6.3 ± 1.6	0.84 ± 0.17	0.9144	Anomalous
L-CS-$GLY_{40}D_{34}$	5.0	25.4 ± 1.5	0.31 ± 0.04	0.9835	Fickian
	7.4	13.3 ± 1.5	0.22 ± 0.08	0.9027	Fickian

The type of diffusion can be inferred from the *n*-coefficient obtained from the Korsmeyer–Peppas model. It can be observed that the L-CS-$GLY_{40}D_7$ sample presented an anomalous diffusion ($0.43 < n < 0.85$) whereas the L-CS-$GLY_{40}D_{34}$ sample showed Fickian diffusion ($n < 0.43$). These results are in agreement with the release profiles observed in Figure 7, suggesting that the L-CS-$GLY_{40}D_7$ sample has larger release due to the anomalous diffusion mechanism. On the other hand, the L-CS-$GLY_{40}D_{34}$ sample has a lower release rate due to more controlled release from the nanoparticles. Therefore, according to the Korsmeyer–Peppas model, the type of release depends on the degree of substitution of the hydrophobic chains. The results indicate that nanoparticles can provide sustained release of QCT over a long period.

Cytotoxicity Assays

The *in vitro* cytotoxicity of free QCT, CS, and its derivatives and QCT-loaded nanoparticles was evaluated by MTT assays. It can be seen in Figure 8(a) that the blank nanoparticles containing L-CS-$GLY_{40}D_7$ and L-CS-$GLY_{40}D_{34}$ showed MCF-7 cell viability higher than 70%. In fact, the cell viability for the derivatives was higher than that for non-modified CS (L-CS), suggesting that amphiphilic samples have improved biocompatibility, especially at the higher concentrations (25 and 50 µg/mL). The decrease in viability with the increase of the C12 chain evidences that the DDA group confers less biocompatibility, confirming that the hydrophobic content is

directly related to the cytotoxic effect. On the other hand, the GLY might be responsible for improving the viability of the amphiphilic samples.

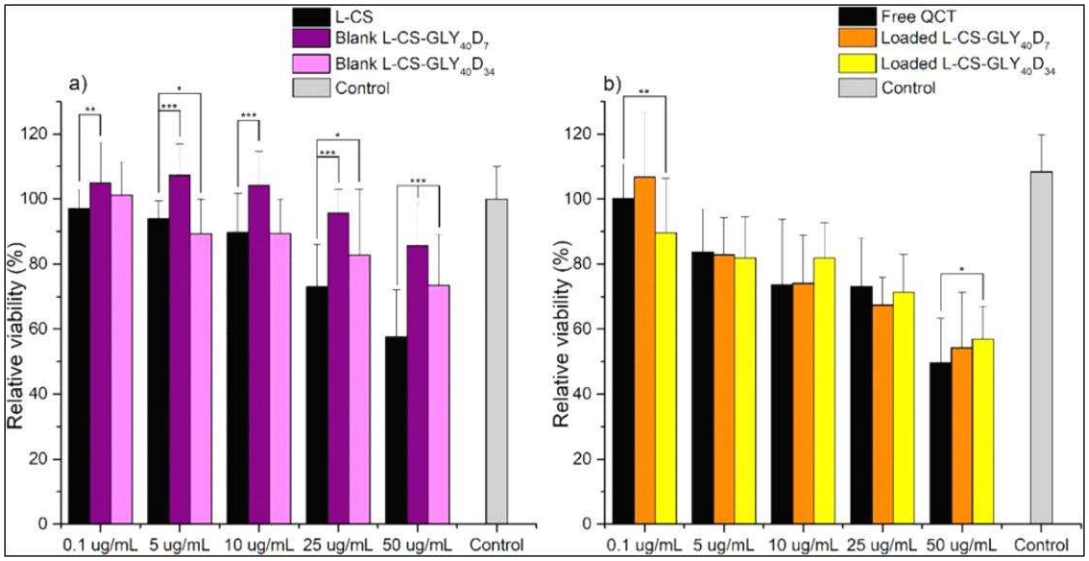

Figure 8
Cytotoxicity of nanoparticles against MCF-7 cells in 96-well plates determined using the MTT assay. (a) Relative cell viability following treatment with L-CS and blank nanoparticles at increasing concentrations. (b) Relative cell viability following treatment with free QCT and QCT-loaded nanoparticles. Absolute concentrations refer to concentration of QCT. For all experiments, cells were incubated for 24 h. Mean values ± SD. (n = 3, ***P < 0.001).

MTT assays were also used to evaluate the antitumor effect of free QCT and the QCT-loaded nanoparticles. Figure 8(b) shows that the reduction of the viability induced by the QCT-loaded nanoparticles was similar to that of the free drug after 24 h, regardless of the fact that only a fraction of the drug was released, as demonstrated by the *in vitro* release experiments. An immediate release of the total amount of QCT loaded into the nanoparticles would have led to a much higher cytotoxic response. The results, however, are in agreement with previous studies. Duo *et al*.60 have shown that QCT works by decreasing the proliferation and inducing apoptosis of MCF-7 cells over time. Recent studies have also showed the effectiveness of QCT against MCF-7 cells.61

Therefore, QCT encapsulation may possibly decrease side effects upon systematic administration due to higher release in the acidic tumor tissue promoted by the amphiphilic carriers. Thus, the nanoparticles pH-sensitivity, sustained release, and the effectiveness of QCT suggest that the carriers studied here can be exploited in cancer therapy.

Blood Compatibility Tests

The blood compatibility of the new materials can be reliably assessed by the erythrocyte-induced hemolysis test.62-64 It is important to ensure that no further interaction with erythrocytes occurs, otherwise it would negatively influence the circulation of the

nanoparticles in the bloodstream. The hemolysis ratio for the L-CS-$GLY_{40}D_7$ and L-CS-$GLY_{40}D_{34}$ samples were 3.2 ± 0.6 and 1.7 ± 0.2, respectively. These results are below the safety limit of 5% for pharmacological applications, suggesting good hemocompatibility.

It has already been shown that CS has a haemolytic tendency.65, 66 This is due to the electrostatic interactions between the positive charges of the polymer and the negative charges of the cell structures. However, modification of the polymer backbone with GLY and DDA groups reduces the surface charges of the particles, improving its hemocompatibility. Similar results have already been reported.67 Biological molecules tend to adsorb on the surface of the particles upon intravenous administration, reducing its ability to damage the erythrocytes in the bloodstream.68 Moreover, the opsonization by serum or plasma proteins, known as opsonize, might also reduce the damage to the erythrocytes caused by the nanoparticles on blood.69

CONCLUSIONS

We have reported here a synthesis of novel amphiphilic derivatives of CS obtained by incorporating GLY and DDA to CS. Solubility experiments showed that insertion of the hydrophilic glycidyl group significantly increases the solubility of the polymer at pH above 6.2. Results showed that CS was easily modified in a successful and controlled reaction to promote self-assembling properties. Fluorescence experiments showed that copolymers self-assemble in aqueous solution at concentrations ranging from 0.003 to 0.047 g/L.

The average size of the nanoparticles ranged from 130 to 300 nm and was dependent on pH, concentration, and hydrophilic/hydrophobic ratio, involving different types of associations among chains. ζ-potential values (+14.1 to +30.4 mV) showed that the particles were positively charged and stable in aqueous solution. TEM images confirmed the spherical morphology of the particles, without significant aggregation among them.

The obtained particles can encapsulate QCT up to 78%. *In vitro* studies showed that the release occurs in two steps, being constant and slow after the initial 8 h, with significant influence of pH. The release mechanism, obtained from the mathematical Korsmeyer–Peppas model, showed dependence on the composition of the sample. Furthermore, the pH sensibility could be used to target specifically the tumour region, increasing the effectiveness of the drug and reducing its impact on health tissues.

Cytotoxicity experiments confirmed that blank nanoparticles were non-cytotoxic. The results further revealed that QCT maintains its effectiveness against MCF-7 cells after encapsulation. The samples showed hemocompatibility, as demonstrated by hemolysis test. Therefore, the glycidyl-dodecyl amphiphilic CS derivatives might be used as pH-sensitive QCT delivery system. The carriers may help in reducing the side effects upon systematic administration of QCT. Thus, the systems developed in this study show biological and physicochemical parameters suitable for applications as a drug carrier.

ACKNOWLEDGMENTS

ROP thanks CAPES (Brazil) and CNPq (200731/2015–7) for Graduate Fellowships and MGN and CCS thank CNPq (Brazil) for a Research Fellowship. Financial support by CNPq (grant 401434/2014–1) is gratefully acknowledged.

REFERENCES

1 Kean, T.; Thanou, M. Adv. Drug. Deliv. Rev. 2010, 62, 3.
2 Du, H. L.; Yang, X. Y.; Pang, X.; Zhai, G. X. Carbohydr. Polym. 2014, 111, 753.
3 Kumar, M. React. Funct. Polym. 2000, 46, 1.
4 Drury, J. L.; Mooney, D. J. Biomaterials 2003, 24, 4337.
5 Dash, M.; Chiellini, F.; Ottenbrite, R. M.; Chiellini, E. Progr. Polym. Sci. 2011, 36, 981.
6 Shrestha, B. K.; Mousa, H. M.; Tiwari, A. P.; Ko, S. W.; Park, C. H.; Kim, C. S. Carbohydr. Polym. 2016, 148, 107.
7 Jayakumar, R.; Prabaharan, M.; Kumar, P. T. S.; Nair, S. V.; Tamura, H. Biotechnol. Adv. 2011, 29, 322.
8 Zhang, D.; Zhou, W.; Wei, B.; Wang, X.; Tang, R. P.; Nie, J. M.; Wang, J. Carbohydr. Polym. 2015, 125, 189.
9 Mao, H. Q.; Roy, K.; Troung-Le, V. L.; Janes, K. A.; Lin, K. Y.; Wang, Y.; August, J. T.; Leong, K. W. J. Control. Release 2001, 70, 399.
10 Jin, L.; Zeng, X.; Liu, M.; Deng, Y.; He, N. Y. Theranostics 2014, 4, 240.
11 Peng, N.; Ai, Z. Y.; Fang, Z. H.; Wang, Y. F.; Xia, Z. P.; Zhong, Z. B. A.; Fan, X. L.; Ye, Q. F. Carbohydr. Polym. 2016, 150, 180.
12 Agnihotri, S. A.; Mallikarjuna, N. N.; Aminabhavi, T. M. J. Control. Release 2004, 100, 5.
13 Soares, P. I. P.; Sousa, A. I.; Silva, J. C.; Ferreira, I. M. M.; Novo, C. M. M.; Borges, J. P. Carbohydr. Polym. 2016, 147, 304.
14 Rabea, E. I.; Badawy, M. E. T.; Stevens, C. V.; Smagghe, G.; Steurbaut, W. Biomacromolecules 2003, 4, 1457.
15 Yan, F. L.; Dang, Q. F.; Liu, C. S.; Yan, J. Q.; Wang, T.; Fan, B.; Cha, D. S.; Li, X. L.; Liang, S. G.; Zhang, Z. Z. Carbohydr. Polym. 2016, 149, 102.
16 Tan, H. L.; Ma, R.; Lin, C. C.; Liu, Z. W.; Tang, T. T. Int. J. Mol. Sci. 2013, 14, 1854.
17 Xing, K.; Shen, X. Q.; Zhu, X.; Ju, X. Y.; Miao, X. M.; Tian, J.; Feng, Z. Z.; Peng, X.; Jiang, J. H.; Qin, S. Int. J. Biol. Macromol. 2016, 82, 830.
18 Hu, L. F.; Meng, X. T.; Xing, R. G.; Liu, S.; Chen, X. L.; Qin, Y. K.; Yu, H. H.; Li, P. C. Bioorg. Med. Chem. Lett. 2016, 26, 4548.
19 Li, K. C.; Xing, R. E.; Liu, S.; Qin, Y. K.; Meng, X. T.; Li, P. C. Int. J. Biol. Macromol. 2012, 51, 767.
20 Larsson, M.; Huang, W. C.; Hsiao, M. H.; Wang, Y. J.; Nyden, M.; Chiou, S. H.; Liu, D. M. Prog. Polym. Sci. 2013, 38, 1307.
21 Barbosa, H. F. G.; Lima, A. M. F.; Taboga, S. R.; Fernandes, J. C.; Tiera, V. A. D.; Tiera, M. J. J. Appl. Polym. Sci. 2016, 133, DOI: 10.1002/app.44176.
22 Mohanty, A. K.; Datta, A.; Venkatraj, V. IEEE Trans. Biomed. Eng. 2014, 61, 966.
23 Maeda, H. Adv. Enzyme Regul. 2001, 41, 189.
24 Bae, Y. H.; Park, K. J. Control. Release 2011, 153, 198.
25 Vaupel, P.; Kallinowski, F.; Okunieff, P. Cancer Res. 1989, 49, 6449.
26 Damaghi, M.; Wojtkowiak, J. W.; Gillies, R. J. Front. Physiol. 2013, 4, 370.
27 Aydin, R. S. T.; Pulat, M. J. Nanomater. 2012, 2012, 1.
28 Rinaudo, M. Prog. Polym. Sci. 2006, 31, 603.

29 Parker, R. E.; Isaacs, N. S. Chem. Rev. 1959, 59, 737.
30 Pedro, R. D.; Schmitt, C. C.; Neumann, M. G. Carbohydr. Polym. 2016, 147, 97.
31 Tiera, M. J.; Qiu, X. P.; Bechaouch, S.; Shi, Q.; Fernandes, J. C.; Winnik, F. M. Biomacromolecules 2006, 7, 3151.
32 Tommeraas, K.; Koping-Hoggard, M.; Varum, K. M.; Christensen, B. E.; Artursson, P.; Smidsrod, O. Carbohydr. Res. 2002, 337, 2455.
33 de Souza, R.; Takaki, M.; Pedro, R. D.; Gabriel, J. D.; Tiera, M. J.; Tiera, V. A. D. Molecules 2013, 18, 4437.
34 Rinaudo, M.; Milas, M.; Ledung, P. Int. J. Biol. Macromol. 1993, 15, 281.
35 Nabid, M. R.; Rezaei, S. J. T.; Sedghi, R.; Niknejad, H.; Entezami, A. A.; Oskooie, H. A.; Heravi, M. M. Polymer 2011, 52, 2799.
36 Korsmeyer, R. W.; Gurny, R.; Doelker, E.; Buri, P.; Peppas, N. A. Int. J. Pharm. 1983, 15, 25.
37 Costa, P.; Manuel, J.; Lobo, S. Eur. J. Pharm. Sci. 2001, 13, 123.
38 Ritger, P. L.; Peppas, N. A. J. Control. Release 1987, 5, 23.
39 Pedro, R. D.; Takaki, M.; Goraye, T. C. C.; Del Bianchi, V. L.; Thomeo, J. C.; Tiera, M. J.; Tiera, V. A. D. Microbiol. Res. 2013, 168, 50.
40 Zhang, A. D.; Ding, D. R.; Ren, J. C.; Zhu, X. L.; Yao, Y. H. J. Appl. Polym. Sci. 2014, 131, DOI: 10.1002/app.39890.
41 Liu, K. P.; Zhang, J. J.; Cheng, F. F.; Zheng, T. T.; Wang, C. M.; Zhu, J. J. J. Mater. Chem. 2011, 21, 12034.
42 Robles, E.; Juarez, J.; Burboa, M. G.; Gutierrez, L. E.; Taboada, P.; Mosquera, V.; Valdez, M. A. J. Appl. Polym. Sci. 2014, 131, 10.
43 Mao, S. R.; Sun, W.; Kissel, T. Adv. Drug Deliv. Rev. 2010, 62, 12.
44 Wu, J.; Wei, W.; Wang, L. Y.; Su, Z. G.; Ma, G. H. Biomaterials 2007, 28, 2220.
45 Thanou, M.; Verhoef, J. C.; Junginger, H. E. Adv. Drug Deliv. Rev. 2001, 52, 117.
46 Iamazaki, E. T.; de Britto, D.; Schmitt, C. C.; Campana, S. P.; Neumann, M. G. Colloid Polym. Sci. 2004, 283, 33.
47 Di Martino, A.; Sedlarik, V. Int. J. Pharm. 2014, 474, 134.
48 Lopez-Leon, T.; Carvalho, E. L. S.; Seijo, B.; Ortega-Vinuesa, J. L.; Bastos-Gonzalez, D. J. Colloid Interface Sci. 2005, 283, 344.
49 Tan, Y-l.; Liu, C.-G. Colloids Surf. B 2009, 69, 178.
50 Yu, B. J.; Tang, C.; Yin, C. H. Biomaterials 2014, 35, 6369.
51 Honary, S.; Zahir, F. Trop. J. Pharm. Res. 2013, 12, 265.
52 Bury, K.; Du Prez, F.; Neugebauer, D. Macromol. Biosci. 2013, 13, 1520.
53 Du, H. L.; Liu, M. R.; Yang, X. Y.; Zhai, G. X. J. Colloid Interface Sci. 2015, 460, 87.
54 Wu, M. M.; Cao, Z. Y.; Zhao, Y. F.; Zeng, R.; Tu, M.; Zhao, J. H. Mater. Sci. Eng. C Mater. Biol. Appl. 2016, 64, 346.
55 Treenate, P.; Monvisade, P. Int. J. Biol. Macromol. 2017, 99, 71.
56 Tiew, S. X.; Misran, M. J. Appl. Polym. Sci. 2017, 134, DOI: 10.1002/app.44849.
57 Islam, M. S.; Haque, P.; Rashid, T. U.; Khan, M. N.; Mallik, A. K.; Khan, M. N. I.; Khan, M.; Rahman, M. M. J. Mater. Sci. Mater. Med. 2017, 28, 55.
58 Hemmati, K.; Alizadeh, R.; Ghaemy, M. Polym. Adv. Technol. 2016, 27, 504.
59 Kaiser, M.; Kirsch, B.; Hauser, H.; Schneider, D.; Seuss-Baum, I.; Goycoolea, F. M. PLoS One 2015, 10, 10.
60 Duo, J.; Ying, G. G.; Wang, G. W.; Zhang, L. Mol. Med. Rep. 2012, 5, 1453.
61 Sarkar, A.; Ghosh, S.; Chowdhury, S.; Pandey, B.; Sil, P. C. Biochim Biophys Acta Gen. Subject. 2016, 1860, 2065.

62 Li, X. Y.; Kong, X. Y.; Zhang, Z. L.; Nan, K. H.; Li, L. L.; Wang, X. H.; Chen, H. Int. J. Biol. Macromol. 2012, 50, 1299.
63 Rao, S. B.; Sharma, C. P. J. Biomed. Mater. Res. 1997, 34, 21.
64 Zhang, C.; Qu, G. W.; Sun, Y. J.; Wu, X. J.; Yao, Z. L.; Guo, Q. L.; Ding, Q. O.; Yuan, S. T.; Shen, Z. L.; Ping, Q. E.; Zhou, H. P. Biomaterials 2008, 29, 1233.
65 Xu, P. S.; Bajaj, G.; Shugg, T.; Van Alstine, W. G.; Yeo, Y. Biomacromolecules 2010, 11, 2352.
66 Baldrick, P. Regul. Toxicol. Pharm. 2010, 56, 290.
67 Huo, M. R.; Zhang, Y.; Zhou, J. P.; Zou, A. F.; Yu, D.; Wu, Y. P.; Li, J.; Li, H. Int. J. Pharm. 2010, 394, 162.
68 Del Pino, P.; Pelaz, B.; Zhang, Q.; Maffre, P.; Nienhaus, G. U.; Parak, W. J. Mater. Horizons 2014, 1, 301.
69 Mogosanu, G. D.; Grumezescu, A. M.; Bejenaru, C.; Bejenaru, L. E. Int. J. Pharm. 2016, 510, 419.